

Technical Note

Typhoon Loss Assessment in Rural Housing in Ningbo Based on Township-Level Resolution

Qiang Li ^{1,2,*} , Hongtao Jia ³, Jun Zhang ¹ , Jianghong Mao ⁴, Weijie Fan ¹, Mingfeng Huang ⁵ and Bo Zheng ⁶

¹ School of Civil Engineering and Architecture, NingboTech University, Ningbo 315100, China; zj@nit.zju.edu.cn (J.Z.); fanwj@nit.zju.edu.cn (W.F.)

² Zhejiang Engineering Research Center for Intelligent Marine Ranch Equipment, Ningbo 315100, China

³ School of Civil Engineering, Chongqing Jiaotong University, Chongqing 400074, China; j906319074@foxmail.com

⁴ College of Architecture & Environment, Sichuan University, Chengdu 610021, China; jhmao@scu.edu.cn

⁵ Institute of Structural Engineering, Zhejiang University, Hangzhou 310058, China; mfhuang@zju.edu.cn

⁶ Ningbo Branch, People's Insurance Company of China, Ningbo 315000, China; zhengbo09@ningbo.picc.com.cn

* Correspondence: liqiang@nit.zju.edu.cn; Tel.: +86-13732253784

Featured Application: According to the high-resolution typhoon loss zoning map of rural housing provided in this paper, local emergency management departments can carry out timely and targeted reinforcement and repair of rural housing in key townships before the typhoon comes to minimize the casualties and economic losses caused by wind collapse.

Abstract: The purpose of this paper was to provide a new approach to achieve quantitative and accurate typhoon loss assessment of disaster-bearing bodies at township-level resolution. Based on the policy insurance data of Ningbo city, this paper took rural housing as the target disaster-bearing body and analyzed the aggregated data of disaster losses such as payout amount and insured loss rate of rural housing in Ningbo area under the influence of 25 typhoons during 2014–2019. The intensity data of disaster-causing factors such as the maximum average wind speed in Ningbo area under the influence of 25 typhoons were simulated and generated with the wind field engineering model, and a township-level high-resolution rural housing typhoon loss assessment model was established using a RBF artificial neural network. It was found that the insured loss rate of rural housing under wind damage was higher in the townships of southern Ningbo than in the townships of northern Ningbo, and the townships with larger insured loss rates were concentrated in mountainous or coastal areas that are prone to secondary disasters under the attack of the typhoon's peripheral spiral wind and rain belt. The RBF neural network can effectively establish a typhoon loss assessment model from the causal factors to the losses of the disaster-bearing bodies, and the RBF neural network has a faster convergence speed and a smaller overall prediction error than the commonly used BP neural network.

Keywords: typhoon; RBF neural network; township-level resolution; loss assessment



Citation: Li, Q.; Jia, H.; Zhang, J.; Mao, J.; Fan, W.; Huang, M.; Zheng, B. Typhoon Loss Assessment in Rural Housing in Ningbo Based on Township-Level Resolution. *Appl. Sci.* **2022**, *12*, 3463. <https://doi.org/10.3390/app12073463>

Academic Editor: Christian W. Dawson

Received: 23 February 2022

Accepted: 28 March 2022

Published: 29 March 2022

Publisher's Note: MDPI stays neutral with regard to jurisdictional claims in published maps and institutional affiliations.



Copyright: © 2022 by the authors. Licensee MDPI, Basel, Switzerland. This article is an open access article distributed under the terms and conditions of the Creative Commons Attribution (CC BY) license (<https://creativecommons.org/licenses/by/4.0/>).

1. Introduction

Ningbo is located in the southeast coast of China and is seriously affected by typhoon disasters every year. For example, the Super Typhoon Lekima hit Ningbo in 2019, causing 408 houses to collapse and damage to 1594 houses citywide. Compared with urban houses, rural houses are less wind-resistant, especially some old houses in disrepair, which are highly susceptible to typhoon damage. Among the existing rural houses in Ningbo, only 14.8% are reinforced concrete houses, 69.9% are brick and concrete houses, and 14.9%, 0.1%, and 0.3% are brick (stone) wooden houses, bamboo and grass adobe houses, and other structures, respectively, according to the data of the third agricultural census in Ningbo (<http://www.cnnb.com.cn/xinwen/system/2018/03/05/008731132.shtml>, accessed on 1 May 2021). Except for the reinforced concrete structure, which has better wind resistance,

houses of brick and concrete, brick and stone, bamboo and grass structures may collapse due to typhoons. Therefore, it is increasingly important to make reasonable disaster loss assessments and predictions for rural housing.

Many scholars in China and abroad have conducted a lot of research on the hazard analysis of typhoon causal factors and vulnerability analysis of disaster-bearing bodies. In the assessment of typhoon causal factors, benefited from the rapid growth of the Monte Carlo method and computer technology, extreme typhoon wind speed simulation has mushroomed in the past twenty years, which is mainly composed of two parts: (1) typhoon track simulation, and (2) wind field simulation. There are two commonly used methods, the circular sub-region method (CSM) and full-track method, which were put forward one after another to serve the typhoon track simulation. Studies in the literature that have indicated the use of CSM to assess the typhoon wind hazards for the coastal region of mainland China or the hurricane wind hazards for the United States have been carried out by Batts et al. [1], Georgiou [2], Vickery and Twisdale [3], Ou et al. [4], Zhao et al. [5], Xiao et al. [6], Li and Hong et al. [7], Hong et al. [8], and Fang et al. [9]. This approach (referred to as the CSM) requires the assignment of probabilistic models for the characteristics of historical track segments within a specified radius of the site of interest such as translational speed, heading, and intensity. However, there could be insufficient historical track data to adequately define the probabilistic models in this approach. To overcome the lack of historical track data, Vickery et al. [10] pioneered a full-track method to generate synthetic hurricane tracks from genesis to lysis based on the historical track records in the National Hurricane Center's North Atlantic hurricane database (HURDAT). The development and utilization of the full-track models for wind hazard assessment have since been considered and expanded (Powell et al. [11]; James and Mason [12]; Emanuel et al. [13]; Lee and Rosowsky [14]; Vickery et al. [15]; Li and Hong [16,17]; Chen and Duan [18]). Li and Hong [16,17] simplified the Vickery's regression model to assess the hurricane/typhoon wind hazards on the U.S. gulf coast and the coastal region of mainland China, respectively. So far, storm tracks can be synthesized rapidly from purely statistical intensity algorithms. However, the effects of natural or anthropogenic climate change could not be encompassed through the above empirical models. Today, some novel intensity models considering environment variables that can be obtained from reanalysis or global climate models have the potential to estimate the future wind hazards under future climate projections. For example, by taking the effects of ocean coupling and environmental wind shear into account, Emanuel [19] presented a fast, physically motivated intensity algorithm and verified the model's validity. Reanalysis data were adopted by Chen and Duan [18] to develop an improved full track model for TCs based on a statistical dynamics method, described as a beta-and-advection model, to estimate wind hazards on the coast of southeast China. Jing and Lin [20] developed a hidden Markov model (MeHiM), which is dependent on the surrounding large-scale environment such as vertical wind shear, relative humidity, and ocean feedback from reanalysis to simulate the whole process of hurricane intensity evolution. Huang et al. [21] verified the applicability of MeHiM in the Northwest Pacific Ocean and presented a general framework of typhoon full-track simulation. For engineering applications, the wind field model can be classified as the gradient wind field model [1,2,14] and the planetary boundary layer (PBL) model [15,16,22]. Meng et al. [22] proposed an analytical model with an upper inviscid layer of cyclostrophic balance and a lower friction layer to calculate the wind field in a moving typhoon boundary layer. Thompson and Cardone [23] upgraded a PBL model by increasing the spatial resolution to simulate a wider variety of radial pressure and wind profile forms. These PBL models have been widely applied in the assessment of hurricane/typhoon wind hazards for the coastal region of the United States and China [5–9,16,17].

In terms of vulnerability analysis of disaster-bearing bodies, Niu et al. [24] analyzed the vulnerability of disaster-bearing bodies in coastal areas of China by considering the characteristics of disaster-causing factors based on natural disaster system theory; Yin et al. [25] assessed the risk of disaster-bearing bodies caused by typhoons in coastal areas of China by establishing an indicator system based on hierarchical analysis; Pielke et al. [26], com-

bined with socioeconomic factors, pointed out that the degree of disaster loss was mainly related to population and economic currency; and Fang et al. [27] established a typhoon vulnerability equation for rural housing in Zhejiang Province using insurance data and provided relevant parameters. Chen et al. [28] established a typhoon disaster prediction model based on comprehensive disaster correlation and typhoon disaster-causing factors; and Lou et al. [29] established a neural network based on the principal component analysis method and used the direct economic loss index as an assessment index for five typhoons in Zhejiang Province.

Up until now, there have been few studies on the typhoon loss assessment of disaster-bearing bodies based on township-level high-resolution due to the scarcity of public information on township-level disaster loss data. The existing studies [24–29] have mainly focused on macro-provincial resolution, which is mainly attributed to the limitation of domestic disaster statistics. Although typhoon disaster statistics in China have made great progress in the past decades, there are still many deficiencies in disaster statistics in different provinces, different generations, and different departments, and the lack of uniform data standards makes it difficult to predict quantitative and accurate disaster losses. At present, emergency management departments around China mainly collect and summarize typhoon disaster data through grassroots disaster informants, and although the data time series is long, there are many human interference factors, the quality of historical data is not ideal, and it focuses on statistics of civil indicators such as the number of affected residents, casualties, and direct economic losses. In addition, the typhoon disaster data provided by meteorological and water conservancy departments have low spatial resolution and mainly focus on disaster-causing factor statistics, lacking disaster-bearing body statistics. Therefore, it is urgent to reconstruct the bottom-up data of disaster-bearing bodies from the county and township levels to provincial and municipal levels for historical typhoon disaster events in China. In recent years, the public catastrophe insurance work carried out by commercial insurance companies can better compensate for the above deficiencies in disaster statistics, the location of insurance targets can be precisely located to townships and villages, and the payout amount can accurately reflect the actual economic losses of the targets, which can be used to quantitatively assess typhoon loss risks. Therefore, this paper used rural housing as the target disaster-bearing body and proposed a new approach to establish a typhoon loss assessment model in rural housing based on township-level resolution by utilizing a RBF neural network with the help of policy insurance data, which can provide a scientific basis for the subsequent formulation of typhoon disaster insurance policies and typhoon emergency plans.

2. Data Sources

The typhoon path and intensity information used in this paper came from the CMA-STI Best Track Dataset for Tropical Cyclones over the western North Pacific compiled by the China Meteorological Administration (CMA) and Shanghai Typhoon Institute (STI). The detailed specification of the CMA-STI Best Track Dataset can be referred to in the work of Ying et al. [30] and the dataset can be obtained from the website (www.typhoon.gov.cn, accessed on 1 May 2021). Based on the screening principle that the typhoon center enters within 500 km of Ningbo meteorological station and the disaster loss information is complete, 25 typhoons affecting Ningbo area during 2014–2019 were selected for analysis, and the specific path information is shown in Figure 1. According to the distance from the typhoon landing site to Ningbo, typhoon paths can be divided into three types: Type I, with landing sites in coastal areas of Zhejiang such as Ningbo and Taizhou; Type II, with landing sites in adjacent provinces and cities such as Fujian and Shanghai; and Type III, with landing sites in more distant areas such as Guangdong or without landing but whose central path entered within 500 km of Ningbo meteorological station.

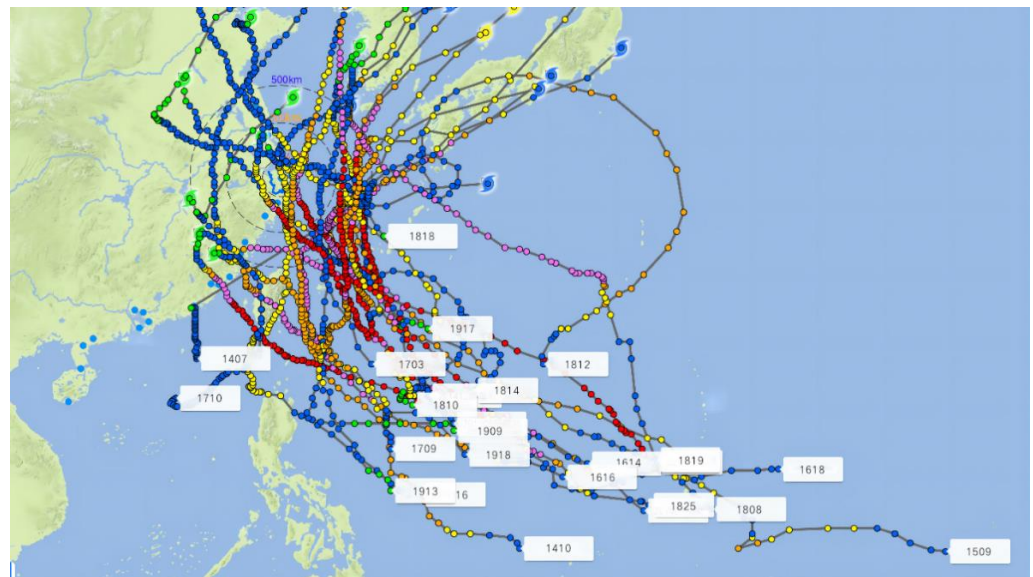


Figure 1. Twenty-five typhoon paths affecting Ningbo area during 2014–2019.

The Ningbo policy rural housing insurance data used in this paper were provided by the Ningbo branch of the People’s Insurance Company (Group) of China Limited. The data include underwriting and claims data. Underwriting data include policy number, number of insured households, underwriting address, insurance amount per household, total insurance premium, etc.; claims data include policy number, date of insurance, reason for insurance, address of insurance, loss of insurance subject, actual compensation amount, etc. The policy number corresponded to each other in the two types of data, and the insurance address detailed the village, town, or street where the accident was located, which can be used to assess the typhoon losses in rural housing in each township.

3. Methods

3.1. RBF Neural Network Fundamentals

The RBF (radical basis function) neural network is an efficient feed-forward network that has the best approximation performance and global optimum properties that other forward networks do not have, and has a simple structure and fast training speed. Its network topology is shown in Figure 2, which contains an input layer, a radial basis function hidden layer, and an output layer. The main advantage is that it can approximate and predict any continuous nonlinear function within arbitrary accuracy and has global approximation capability, which fundamentally solves the local optimum problem of the BP neural network, the topology is compact, and the structural parameters can be separated for learning [31]. In addition, the generalization ability of the RBF network is also better than the BP network in several aspects. In the RBF neural network, the input data enter the input layer without any transformation. When the data enter the hidden layer, the hidden layer neural nodes perform a kind of spatial nonlinear mapping transformation on the data through the basis function. The output layer uses a linear optimization strategy, so the learning speed can be faster. Finally, the mapped values are output by a linearly weighted combination of the output layer neural nodes.

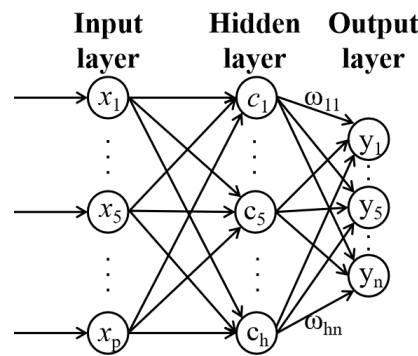


Figure 2. RBF neural network structure.

The input layer of RBF neural network realizes the spatial nonlinear mapping transformation $x_p \rightarrow R(x_p - c_i)$ by a radial basis function, where the commonly used basis functions are Gaussian functions with the following activation functions:

$$R(x_p - c_i) = \exp\left(-\frac{1}{2\sigma^2} \|x_p - c_i\|^2\right) \tag{1}$$

where $\|x_p - c_i\|$ is the Euclidean norm; $x_p = (x_1^p, x_2^p, \dots, x_m^p)^T$ representing the p th input data; c_i is the implicit layer node center; and σ is the variance of the basis function.

The output layer of the RBF neural network achieves a linear mapping $R(x_p - c_i) \rightarrow y_j$ by weighted combinations, denoted as:

$$y_j = \sum_{i=1}^h \omega_{ij} R(x_p - c_i) \quad j = 1, 2, \dots, n \tag{2}$$

where ω_{ij} is the connection weight from the implicit layer to the output layer; $i = 1, 2, 3, \dots, h$, h is the number of nodes in the hidden layer; and y_j is the j th actual output value corresponding to the data.

3.2. BP Neural Network Fundamentals

The BP (back propagation) neural network is a multilayer feedforward network trained according to the error back propagation algorithm and is one of the most widely used neural network models, whose network structure is shown in Figure 3. The standard BP network generally consists of three neuron layers: the input layer, the hidden layer, and the output layer, and the neurons in the layers form a fully interactive connection with each other, and the neurons within the layers are independent of each other. The BP neural network algorithm is based on the error between the true value and the output value, and adjusts its weights and threshold values backward to finally achieve the minimum mean square error. Since the learning speed of BP neural network is fixed, the network converges slowly and requires a long training time.

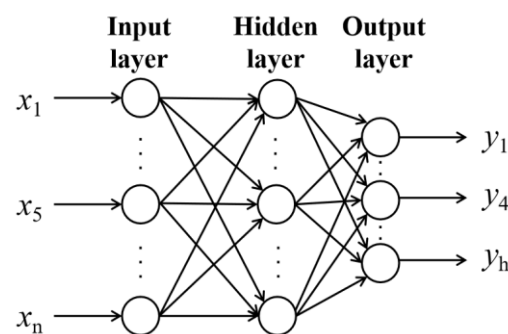


Figure 3. BP neural network structure.

3.3. Construction of Typhoon Loss Assessment Model for Rural Housing

The flow chart for the construction of a typhoon loss assessment model for rural housing is shown in Figure 4. As can be seen, the simulated typhoon wind speed was selected as input layer data, and the output layer data were the insured loss rate of each township due to typhoons, and the statistical data covered 139 townships in Ningbo. Based on the available data of the typhoon causal factors and the losses of the disaster-bearing bodies, the typhoon loss assessment models of rural housing based on the RBF neural network and BP neural network can be established, respectively. Among them, the construction of the RBF neural network is simpler than a BP neural network. Based on the existing data samples, a neural network with a radial basis function expansion factor of 1.2 was created by the “newrb” function, and the mean square error target was set to 0.001. The training algorithm of RBF neural network can be divided into two steps: the first step is to decide the number of nodes in the hidden layer and the center c_i of the basis function according to the distribution of training samples; and the second step is to obtain the connection weights ω_{ij} based on the determined network parameters.

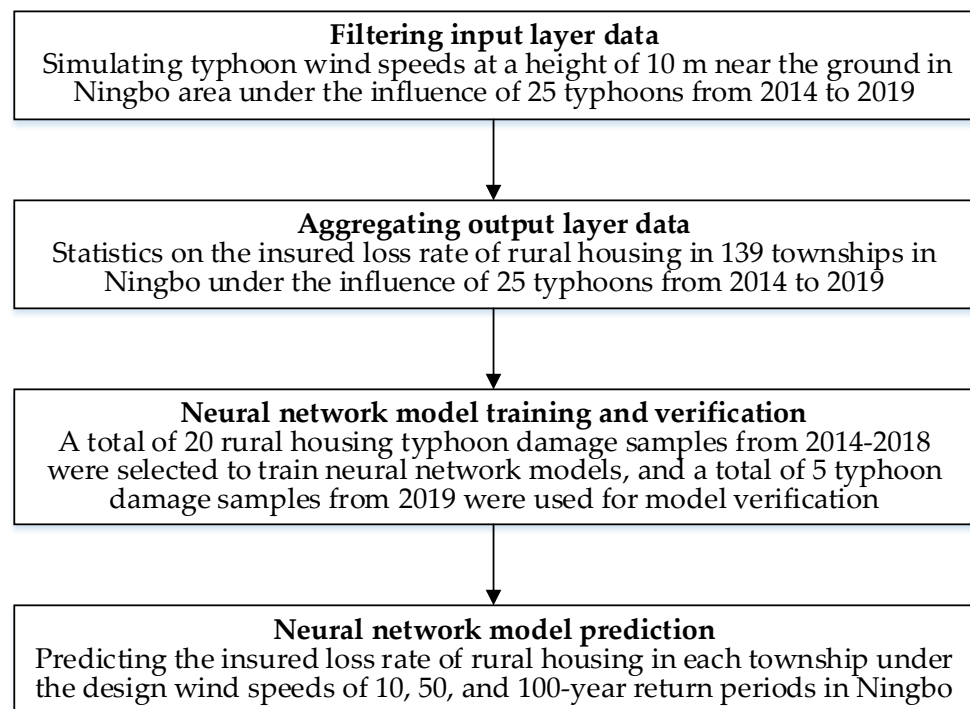


Figure 4. The flow chart for construction of typhoon loss assessment model for rural housing in Ningbo.

The BP neural network was designed as a typical 3-layer network model. The number of neurons in the hidden layer was determined as five by the empirical formula and trial-and-error method, and the transfer functions were tangent S-type transfer function “tansig” and linear transfer function “purelin”, respectively. The system default “trainlm” function was used for training, and the training number was set to 1000, the training target was 0.001, and other parameters were taken as default values.

4. Results

4.1. Typhoon Characteristics and Wind Field Simulation

The daily wind speed data of Ningbo ground meteorological stations (58,562 Yinzhou and 58,467 Cixi) were extracted from the China Meteorological Data System (CMDS) (<http://data.cma.cn/>, accessed on 1 May 2021). According to the meteorological data specification, the collected wind speed data were carefully calibrated by adjusting the observation height, observation time interval, and so on, to the standard condition. However, it was found that the daily maximum 10 min average wind speeds observed at the meteo-

rological stations during the typhoon strike were small, so additional numerical simulation of the typhoon wind field was needed. The reason for the low observed typhoon wind speeds may be due to the change of the terrain near the meteorological station. Attributable to the rapid urbanization in China since the 1980s, the terrain near the meteorological station might have changed dramatically so that the exposure category in the vicinity of the original anemometer site might become very different from the initial open rural exposure [32]. Therefore, it is questionable to directly utilize the observed wind speed series to represent true typhoon wind speeds near the ground. In this paper, the Yan Meng wind field model [22] was used to simulate the near-surface typhoon wind speeds in the Ningbo area. The schematic diagram of the activating wind field model is shown in Figure 5. The Vickery empirical model [33] was used to determine the values of key wind field parameters such as the maximum wind speed radius R_{max} and Holland pressure profile parameter B . The roughness length was taken as 0.05 m. The 10 min average maximum wind speeds at a height of 10 m near the ground in the Ningbo area under the influence of 25 typhoons were obtained by wind field simulation. The specific characteristics of 25 typhoons are shown in Table 1. From Table 1, it can be seen that the simulated typhoon wind speeds were larger than the observed wind speeds. The average number of typhoons affecting the Ningbo area is four to five per year from 2014 to 2019. Among these, type I typhoons that landed on the coast of Zhejiang and caused serious impacts on Ningbo occurred on average one time per year. The 25 selected typhoons affected Ningbo for three to four days on average, with the shortest lasting effect of only one day (Typhoon Mitag 1918) and the longest lasting effect of eight days (Typhoon Jongdari 1812).

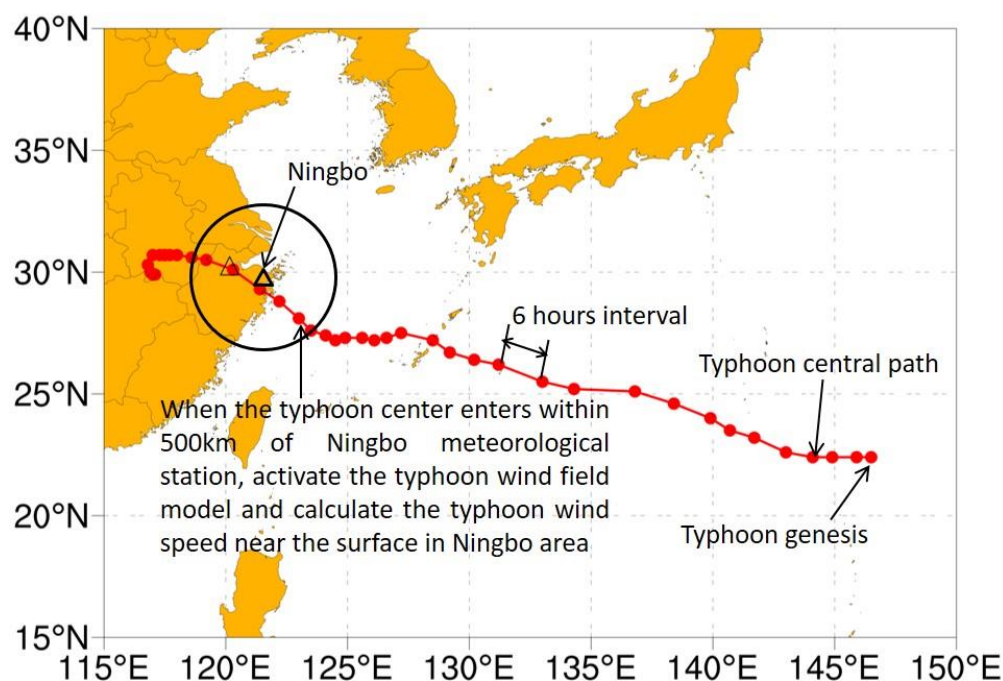


Figure 5. Schematic diagram of the activating wind field model.

Table 1. Specific characteristics of 25 typhoons affecting the Ningbo area.

Year	Impact Time (Month/Day)	Typhoon Number and Name	Landing Location	Path Type	(Meteorological Station Observation) 10 min Average Maximum Wind Speed in Ningbo (m/s)	(Yan Meng Wind Field Model) 10 min Average Maximum Wind Speed in Ningbo (m/s)
2014	6/15–6/17	1407 Hagibis	Shantou, Guangdong	Type III	6.3	5.3
2014	7/8–7/9	1408 Neoguri	Not landed in China	Type III	6.4	7.6
2014	7/23–7/27	1410 Matmo	Taiwan; Fuzhou, Fujian	Type II	7.8	8.6
2014	8/1–8/2	1412 Nakri	Not landed in China	Type III	6.0	8.4
2014	9/21–9/24	1416 Fung-wong	Taiwan; Ningbo, Zhejiang	Type I	7.9	18.4
2015	7/9–7/13	1509 Chan-hom	Zhoushan, Zhejiang	Type I	9.0	33.0
2016	9/12–9/16	1614 Meranti	Xiamen, Fujian	Type II	5.8	6.2

Table 1. Cont.

Year	Impact Time (Month/Day)	Typhoon Number and Name	Landing Location	Path Type	(Meteorological Station Observation) 10 min Average Maximum Wind Speed in Ningbo (m/s)	(Yan Meng Wind Field Model) 10 min Average Maximum Wind Speed in Ningbo (m/s)
2016	9/16–9/17	1616 Malakas	Not landed in China	Type III	9.2	10.9
2016	10/3–10/5	1618 Chaba	Not landed in China	Type III	8.5	3.8
2017	7/2–7/4	1703 Nanmadol	Not landed in China	Type III	9.7	6.0
2017	7/27–7/30	1709 Nesat	Taiwan; Fuqing, Fujian	Type II	6.3	5.0
2017	7/31–8/2	1710 Haitang	Taiwan; Fuqing, Fujian	Type II	7.7	5.6
2017	9/13–9/17	1718 Talim	Not landed in China	Type III	8.4	11.4
2018	7/9–7/11	1808 Maria	Lianjiang, Fujian	Type II	9.3	11.5
2018	7/21–7/23	1810 Ampil	Shanghai	Type II	7.9	20.1
2018	7/26–8/03	1812 Jongdari	Shanghai	Type II	9.5	23.1
2018	8/10–8/14	1814 Yagi	Wenling, Zhejiang	Type I	7.5	19.2
2018	8/16–8/19	1818 Rumbia	Shanghai	Type II	8.4	22.2
2018	8/22–8/23	1819 Soulik	Not landed in China	Type III	6.0	9.5
2018	10/4–10/6	1825 Kong-rey	Not landed in China	Type III	11.0	4.6
2019	7/17–7/19	1905 Danas	Not landed in China	Type III	7.0	6.6
2019	8/9–8/11	1909 Lekima	Wenling, Zhejiang	Type I	12.3	28.2
2019	9/6–9/7	1913 Lingling	Not landed in China	Type III	8.8	12.6
2019	9/21–9/22	1917 Tapah	Not landed in China	Type III	9.8	5.4
2019	10/1–10/3	1918 Mitag	Zhoushan, Zhejiang	Type I	15.5	32.4

4.2. Typhoon Loss Statistics in Rural Housing in Ningbo

The insured loss rate of rural housing in each township under the influence of different typhoon paths from 2014 to 2019 was counted, and representative typhoons were selected for analysis, as shown in Figures 6–8. Combined with the typhoon wind speed data in Table 1, it can be seen that the disaster losses of rural housing in the Ningbo area under the influence of different typhoon paths varied greatly. In general, the insured loss rate of townships and the wind speed of typhoons affecting Ningbo area were positively correlated. Specifically, typhoons landing on the coast of Zhejiang (i.e., type I typhoons such as 1509 Typhoon Chan-hom and 1909 Typhoon Lekima) caused more damage to rural houses in Ningbo area than typhoons landing in neighboring provinces and cities such as Fujian (i.e., type II typhoons). Type III typhoons such as 1616 Typhoon Malakas, although they did not make landfall in China and the affected typhoon wind speeds in Ningbo were small, the typhoon centers entered within the 500 km range of Ningbo during their evolution and still caused great damage to the rural houses in Ningbo townships. The main reason is that under the attack of the typhoon’s peripheral spiral wind and rain belt, secondary disasters such as floods, landslides, and mudslides occurred in the mountainous areas of Ningbo, and rural housing was highly susceptible to damage from secondary disasters.

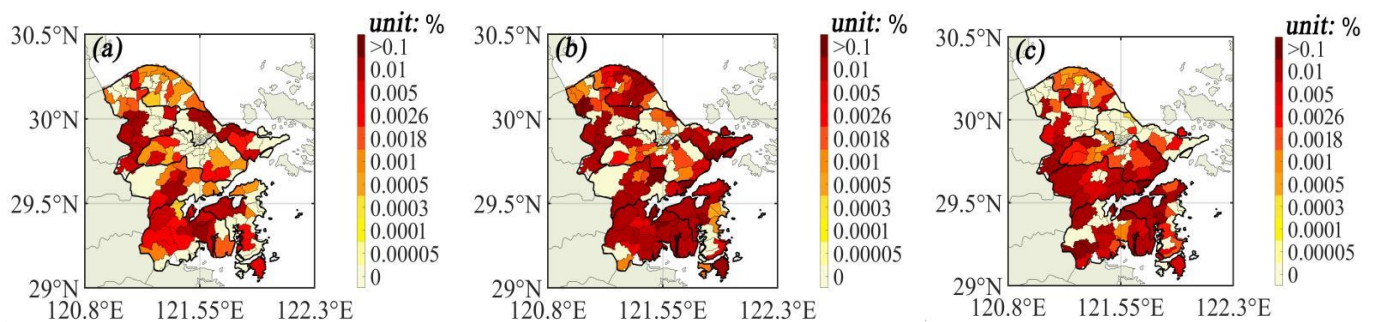


Figure 6. Insured loss rate of townships due to type I typhoons. (a) 1416 Fung-wong; (b) 1509 Chan-hom; (c) 1909 Lekima.

A summary of the underwriting data and claims data due to typhoons from 2014–2019 according to district and county scales (as shown in Table 2) showed that the 6-year total coverage varied widely among districts and counties, and the total coverage was significantly higher in Cixi than in other districts and counties due to the largest population base. The zoning map of Ningbo districts and counties is shown in Figure 9. As can be seen from Table 2, Yuyao, Xiangshan, Ninghai, and Cixi had a higher total payout amount, and Xiangshan, Beilun, Ninghai, Yuyao had larger insured loss rates. It is worth mentioning that

in the insurance claims data, “fire”, “rainstorm”, “accident”, and other factors accounted for the majority of the insurance records, while typhoons only accounted for a small percentage of the insurance records. Therefore, the overall value of the insured loss rate caused by typhoons is small. Second, it is also common that the cause of insurance was not clearly marked, and the insurance estimator only marked “typhoon” when marking the cause of insurance, while other secondary disasters such as landslides, floods, and mudslides caused by typhoons were not recorded, resulting in some claims records not corresponding to the specific typhoon causal factors, and therefore, the total payout amount will be omitted in the statistics. The overall average insured loss rate was 0.00106%.

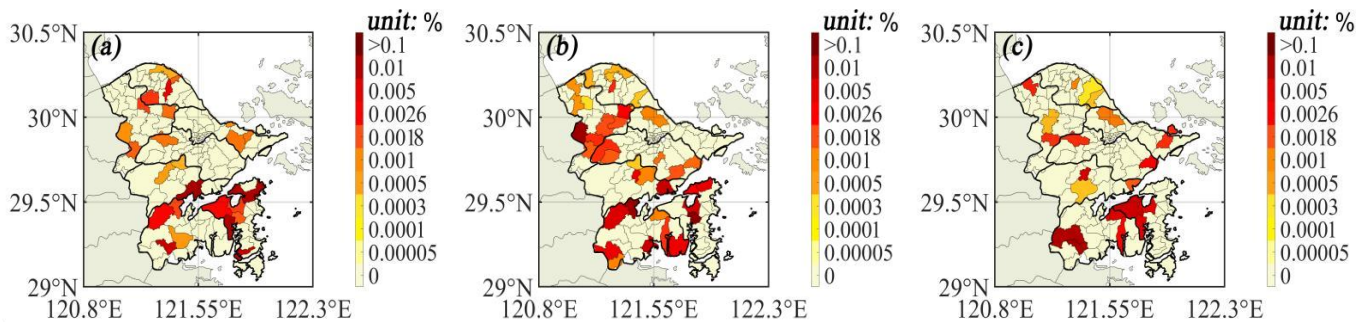


Figure 7. Insured loss rate of townships due to type II typhoons. (a) 1410 Matmo; (b) 1614 Meranti; (c) 1808 Maria.

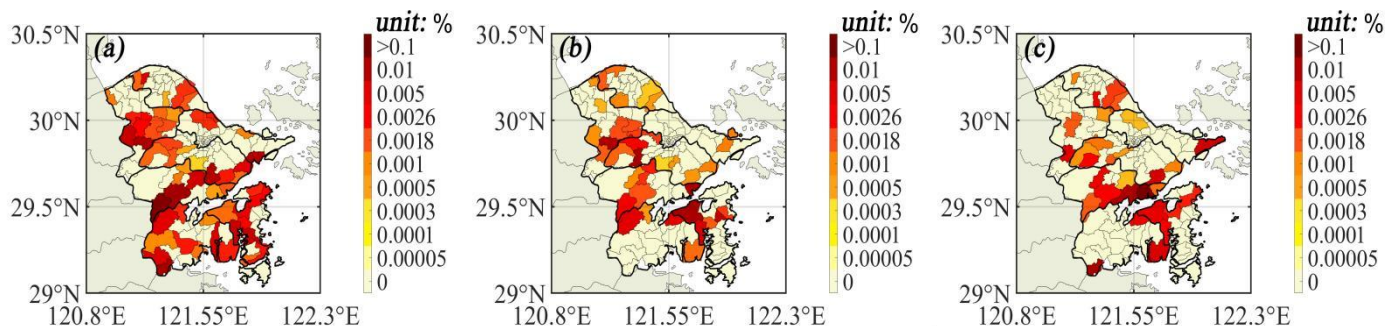


Figure 8. Insured loss rate of townships due to type III typhoons. (a) 1616 Malakas; (b) 1618 Chaba; (c) 1718 Talim.

Table 2. Summary of insurance claims for rural housing in the Ningbo districts and counties caused by typhoons.

District and County	6-Year Total Payout (¥)	6-Year Total Coverage (¥)	Insured Loss Rate	The Township with the Largest Insured Loss Rate
Beilun	188,000	11,336,218,951	0.00166%	Meishan Township (0.007252%)
Cixi	309,000	60,500,740,600	0.00051%	KuangYan Township (0.001439%)
Fenghua	152,600	23,526,372,972	0.00065%	Shangtian Township (0.001381%)
Haishu	183,600	21,288,276,900	0.00086%	Hengjie Township (0.00474%)
Jiangbei	48,000	5,741,707,313	0.00084%	Hongtang Street (0.001141%)
Ninghai	382,049	25,547,294,750	0.00150%	Chayuan Township (0.003258%)
Xiangshan	393,900	20,265,580,500	0.00194%	Maoyang Township (0.009984%)
Yinzhou	145,950	26,797,96,800	0.00054%	Jungi Township (0.001853%)
Yuyao	543,400	37,188,688,850	0.00146%	Luting Township (0.009502%)
Zhenhai	53,035	7,841,041,500	0.00068%	Luotuo Street (0.001003%)
Average insured loss rate			0.00106%	

In order to more visually analyze the impact of typhoon disasters on rural housing in each township in Ningbo, Figure 10 shows the zoning map of the total insured loss rate of rural housing in each township due to typhoons from 2014 to 2019. Combined with Table 2, it can be seen that Ningbo Xiangshan County, which is a place where typhoons have landed many times historically, had the largest insured loss rate amongst the Ningbo

districts and counties, and the insured loss rate of Maoyang Township within Xiangshan County was close to 0.01%. In addition, the insured loss rate of Beilun, Ninghai, and Yuyao counties was higher than the average value in Ningbo, with the largest loss rate of Meishan Township in Beilun, Chayuan Township in Ninghai, and Luting Township in Yuyao being 0.007252%, 0.003258%, and 0.009502%, respectively. The rural houses in these townships are mainly of a brick (stone) mixed structure, and such structural systems find it difficult to resist the strong wind and rain impact brought by typhoons. Therefore, the insured loss rate in these areas is larger, and rural houses have a greater risk of damage.

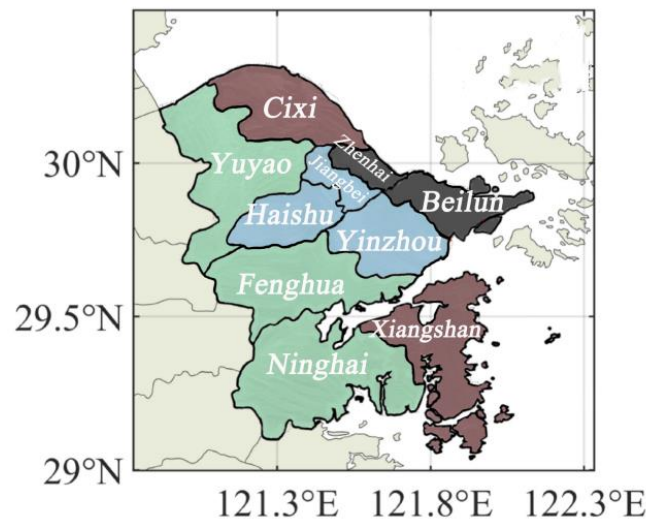


Figure 9. Zoning map of Ningbo districts and counties.

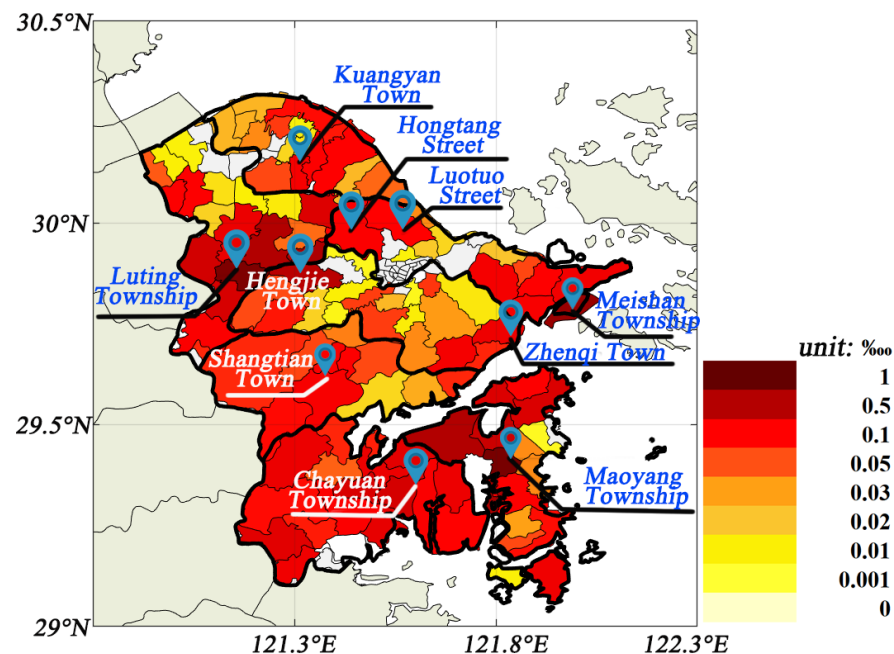


Figure 10. Total insured loss rate of rural housing due to typhoons by townships in Ningbo (2014–2019).

4.3. Model Training and Verification

A total of 20 rural housing typhoon damage samples from 2014–2018 were selected to train the RBF and BP neural network models, and a total of five typhoon damage samples from 2019 were used for model verification. The predicted values of the BP model were used for comparison. During the training process of the RBF neural network, the number of nodes in the hidden layer can be automatically increased until it reaches the maximum

number of nodes in the hidden layer or the accuracy requirement. In the BP neural network training process, in order to make the output results closer to the training target, it is necessary to debug the number of nodes in the hidden layer within the model, the training function, and other related parameters for a long time. When the neural network model is trained, the corresponding training curve can be obtained, as shown in Figure 11. As can be seen from the figure, when the training accuracy was set to 0.001, both models converged under the given conditions, and the BP neural network model needed 110 steps to reach the accuracy requirement. The RBF neural network model required only 12 steps to achieve the same condition, and its training speed was significantly better than that of the BP neural network. The above analysis shows that the RBF neural network has more advantages over the BP neural network in the training speed.

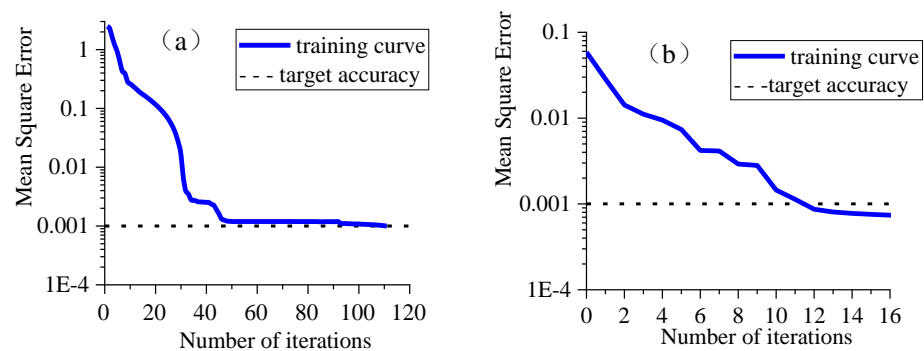


Figure 11. Model training curve. (a) BP neural network. (b) RBF neural network.

To calibrate the models, the predicted values of the BP and RBF neural network models were compared with the actual values (i.e., the average insured loss rate of rural housing under the impact of five typhoons in 2019) and the mean square error was used as the evaluation indicator. The results are shown in Figures 12 and 13. A total of 139 townships in Ningbo were numbered sequentially. It can be seen that both two models could accurately predict the insured loss rate for most townships. However, due to the single input typhoon causal factor (i.e., simulated typhoon wind speed) and the small training sample size (i.e., 20 typhoon damage samples), the two models were less effective in predicting some townships with sudden changes in insured loss rates. In addition, both the BP model and the RBF model had a limited prediction effect for the townships with 0 insured loss rate. Therefore, the predicted values of insured loss rate for some townships were overestimated. In Figure 13, it is noteworthy that the maximum mean square error of the BP model was 18×10^{-6} , which was less accurate and had a larger fluctuation in the error range than the RBF model with a maximum mean square error of 8×10^{-6} . Overall, the mean square error of the predicted values of the RBF neural network was smaller than that of the BP neural network.

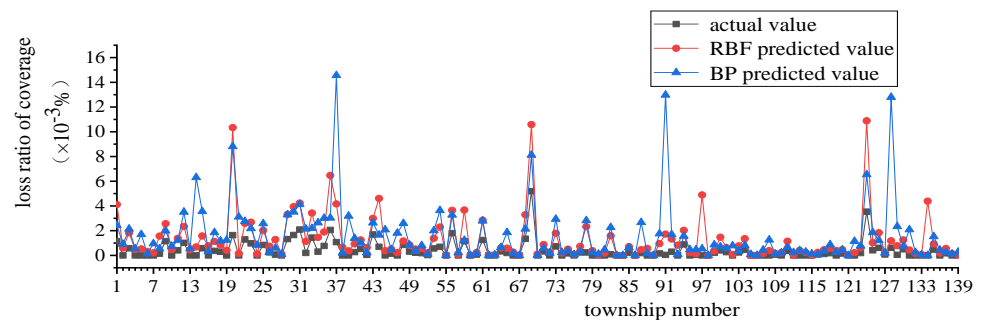


Figure 12. Comparison of average insured loss rate by township due to five typhoons in 2019.

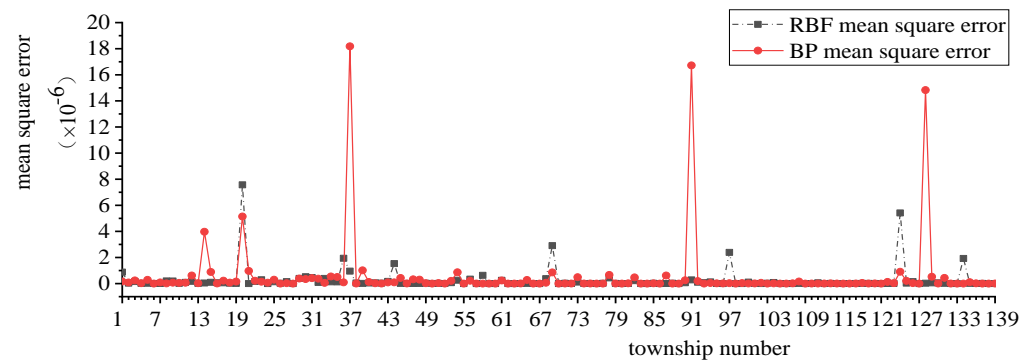


Figure 13. Comparison of mean square error of prediction results between the BP and RBF models.

In order to compare the prediction accuracy of the RBF and BP neural network models more intuitively, the data in Figure 12 were visualized and the zoning maps are shown in Figure 14. In the figure, the RBF prediction results were basically consistent with the actual situation, while in contrast, the BP prediction results had obvious errors with the actual situation; in particular, some townships in the highlighted circles in Figure 14 failed to achieve the loss prediction effect. The most severely affected townships obtained from Table 2 were selected for comparative analysis (see Table 3). According to the comparison, although problems such as small sample size led to some deviations between the predicted values and the actual values in each township, the errors in the predicted values of the RBF model were smaller than those of the BP model in most of the severely affected townships. The results showed that the RBF neural network model is more advantageous than the BP model in reflecting the change in the average insured loss rate of rural houses in each township for the purpose of disaster loss assessment.

4.4. Model Prediction

The trained RBF neural network model can be used to predict the insured loss rate of rural housing in each township under different design wind speeds in Ningbo. The corresponding design wind speeds in Ningbo (input layer data) were calculated according to the wind pressures of 10, 50, and 100 year return periods as specified in the current Building Structure Load Code (GB50009-2012) [34], and their values were 21.9 m/s, 28.3 m/s, and 31.0 m/s, respectively. The output layer results are shown in Figure 15. Overall, the RBF neural network model showed a positive correlation between the insured loss rate of rural housing and the design wind speeds (i.e., the higher the wind speed, the higher the disaster loss). Under the same design wind speed, the insured loss rate of rural houses in the townships of Fenghua District, Ninghai County, and Xiangshan County in the south of Ningbo was much higher than that in the northern townships. Under the design wind speed of a 100-year return period (31.0 m/s), the insured loss rate of rural housing in more than 100 out of 139 townships would be greater than 0.1%, which indicates that rural houses in Ningbo will suffer great damage. According to the above quantitative typhoon loss prediction results, the local emergency management bureau can carry out timely and targeted reinforcement and repair of rural housing in key townships before the typhoon arrives to minimize casualties and economic losses caused by wind collapse.

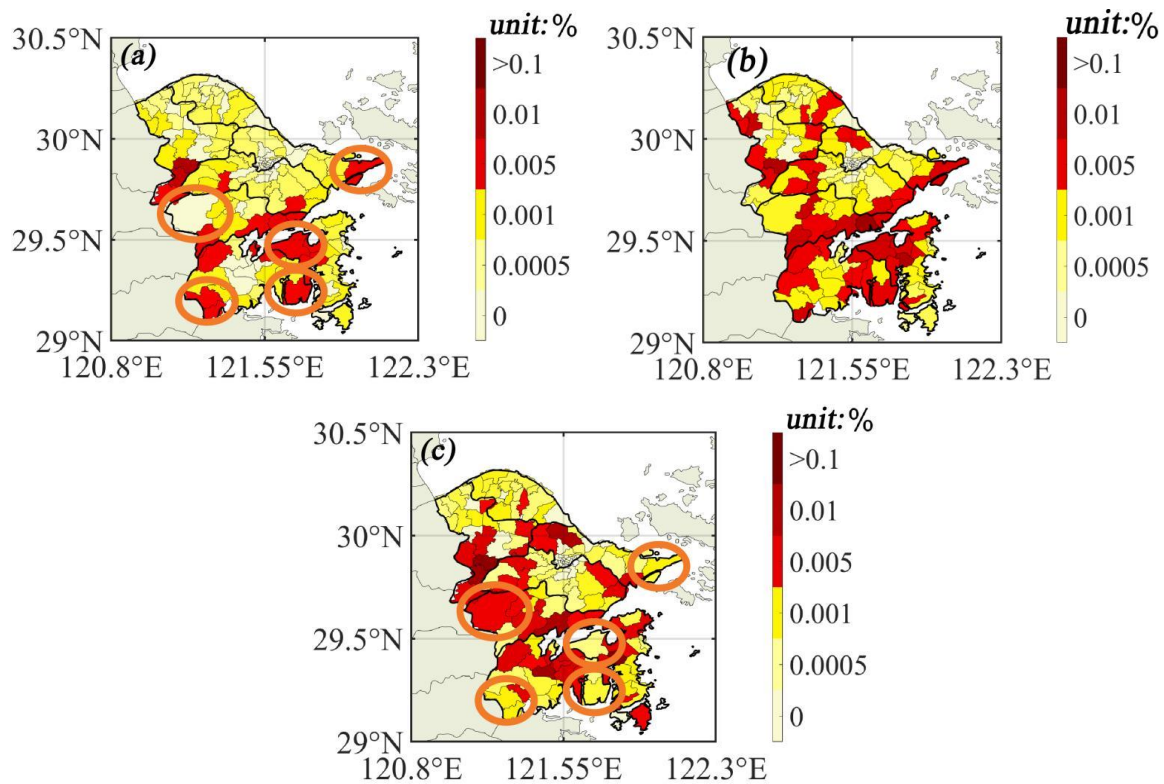


Figure 14. Average insured loss rate by township due to five typhoons in 2019. (a) Actual value; (b) RBF prediction; (c) BP prediction.

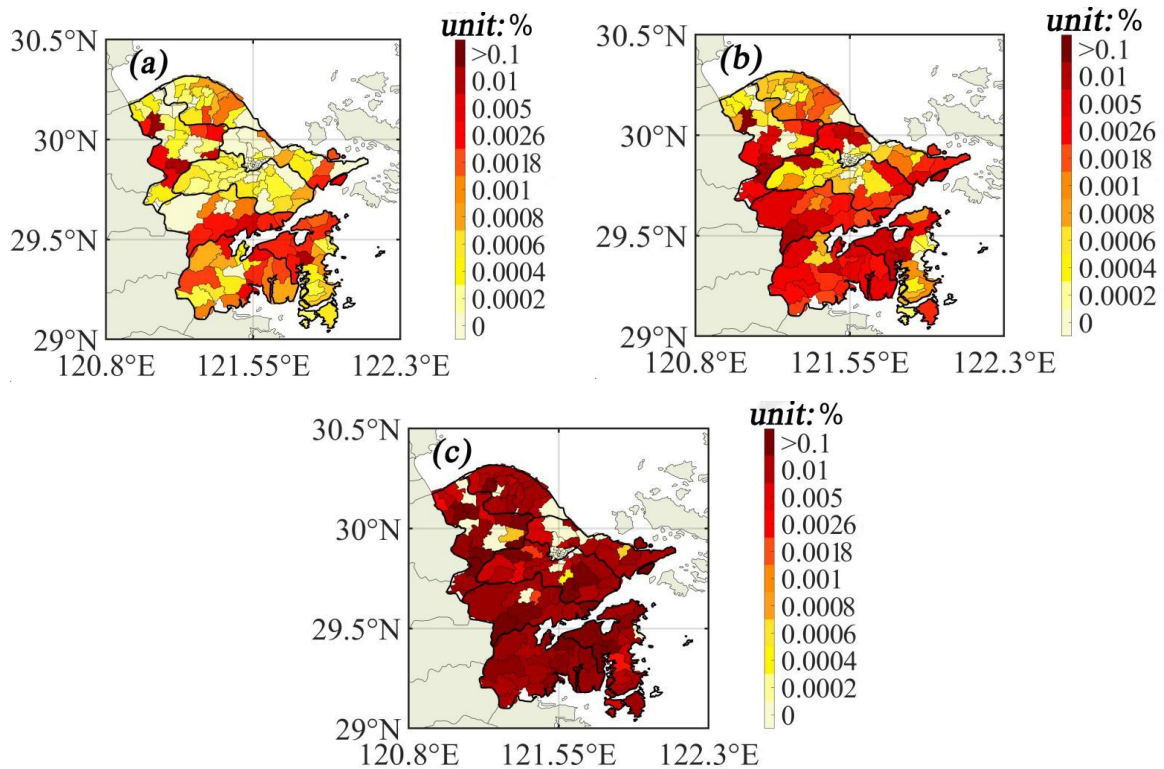


Figure 15. RBF neural network prediction results. (a) Loss rate under the design wind speed of 10 year return period (21.9 m/s); (b) Loss rate under the design wind speed of 50 year return period (28.3 m/s); (c) Loss rate under the design wind speed of 100 year return period (31.0 m/s).

Table 3. Average insured loss rates in 2019 for rural housing in the most severely affected townships.

Township Number	Township Name	Actual Value ($\times 10^{-2}$)	RBF Predicted Value ($\times 10^{-2}$)	RBF Error Value ($\times 10^{-2}$)	BP Predicted Value ($\times 10^{-2}$)	BP Error Value ($\times 10^{-2}$)
4	Kuangyan Town	0.097%	0.103%	0.006%	0.090%	0.007%
15	Chayuan Township	0.058%	0.026%	0.032%	0.356%	0.298%
24	Maoyang Township	0.106%	0.095%	0.011%	0.023%	0.083%
35	Luotuo Street	0.077%	0.156%	0.079%	0.302%	0.225%
37	Shangfian Town	0.098%	0.416%	0.318%	1.456%	1.358%
47	Meishan Township	0.103%	0.080%	0.023%	0.283%	0.180%
48	Zhenqi Town	0.085%	0.054%	0.031%	0.259%	0.174%
69	Luting Township	0.519%	1.058%	0.539%	0.812%	0.293%
73	Hengjie Town	0.073%	0.039%	0.034%	0.270%	0.197%
87	Hongtang Street	0.096%	0.069%	0.027%	0.345%	0.249%

5. Conclusions

This paper proposed a new approach to achieve quantitative and accurate typhoon loss assessment of disaster-bearing bodies at township-level high-resolution. The rural housings in Ningbo area were taken as the target disaster-bearing bodies and a typhoon loss assessment model in rural housing based on township-level resolution was established by utilizing the RBF neural network with the help of public catastrophe insurance data. The specific findings are as follows:

- (1) The RBF neural network could effectively establish a typhoon loss assessment model from the causal factors to the losses of the disaster-bearing bodies, and the RBF neural network converged faster and had a smaller overall prediction error compared to the commonly used BP neural network.
- (2) Overall, the insured loss rate of rural housing due to typhoons showed a positive correlation with the typhoon wind speed affecting Ningbo area. Under the impact of typhoon disaster, the insured loss rate of rural housing was higher in the townships of southern Ningbo than in the townships of northern Ningbo. The townships with larger insured loss rates were concentrated in mountainous and coastal areas that are prone to secondary disasters under the attack of the typhoon's peripheral spiral wind and rain belt.

It should be noted that although the typhoon loss assessment model for rural houses proposed in this paper was well applied in most townships in Ningbo, there were still a few townships where the predicted value of insured loss rate decreased with the increase in design wind speed, and even the situation of 0 insured loss rate exists. In order to further improve the model prediction accuracy, subsequent improvements can be made in terms of increasing the model input layer variables and improving the completeness of insurance claim records. For example, the model can be improved by adding typhoon rainfall, typhoon central pressure, distance from typhoon landfall to target site, and other disaster-causing factors as model inputs. In addition, the insurance loss estimator should clearly distinguish typhoon disaster-causing factors and secondary disasters such as strong wind, heavy rain, landslide, flood, mudslide, etc. when making notes on the cause of the subject matter.

Since the RBF neural network-based typhoon loss assessment model for disaster-bearing bodies proposed in this paper was purely data-driven, future research work will build on this research to analyze the structural vulnerability and damage mechanisms of disaster-bearing bodies under extreme typhoon loads by establishing physical finite element models for disaster-bearing bodies, and then establish a link with economic losses to finally realize a physically-driven quantitative typhoon loss assessment model for disaster-bearing bodies.

Author Contributions: Conceptualization, Q.L.; Writing—original draft preparation, H.J.; Writing—review and editing, Q.L.; Supervision, J.Z., J.M., W.F., M.H., and B.Z. All authors have read and agreed to the published version of the manuscript.

Funding: This research was funded by National Natural Science Foundation of China (51908496, 51820105012), Natural Science Foundation of Zhejiang Province and Ningbo City (LQ20E080001, 2021J168) and Science and Technology Special Project of Ningbo Fenghua District (202008502).

Institutional Review Board Statement: Not applicable.

Informed Consent Statement: Not applicable.

Data Availability Statement: Some or all data and models that support the findings of this study are available from the corresponding author upon reasonable request.

Acknowledgments: We thank the Ningbo branch of the People's Insurance Company of China for providing the necessary data support for this study.

Conflicts of Interest: The authors declare no conflict of interest.

References

1. Batts, M.E.; Simiu, E.; Russell, L.R. Hurricane Wind Speeds in the United States. *J. Struct. Div.* **1980**, *106*, 2001–2016. [[CrossRef](#)]
2. Georgiou, P.N. Design Wind Speeds in Tropical Cyclone-Prone Regions. Ph.D. Thesis, University of Western Ontario, London, ON, Canada, 1985.
3. Vickery, P.J.; Twisdale, L.A. Wind-Field and Filling Models for Hurricane Wind-Speed Predictions. *J. Struct. Eng.* **1995**, *121*, 1700–1709. [[CrossRef](#)]
4. Ou, J.P.; Duan, Z.D.; Chang, L. Typhoon risk analysis for key coastal cities in southeast China. *J. Nat. Disaster* **2002**, *11*, 9–17. (In Chinese)
5. Zhao, L.; Ge, Y.J.; Xiang, H.F. Application of typhoon stochastic simulation and its extreme value wind prediction. *J. Tongji Univer. Nat. Sci.* **2005**, *33*, 885–889. (In Chinese)
6. Xiao, Y.F.; Duan, Z.D.; Xiao, Y.Q.; Ou, J.P.; Chang, L.; Li, Q.S. Typhoon wind hazard analysis for southeast China coastal regions. *Struct. Saf.* **2011**, *33*, 286–295. [[CrossRef](#)]
7. Li, S.H.; Hong, H.P. Use of historical best track data to estimate typhoon wind hazard at selected sites in China. *Nat. Hazards* **2014**, *76*, 1395–1414. [[CrossRef](#)]
8. Hong, H.P.; Li, S.H.; Duan, Z.D. Typhoon Wind Hazard Estimation and Mapping for Coastal Region in Mainland China. *Nat. Hazards Rev.* **2016**, *17*, 04016001. [[CrossRef](#)]
9. Fang, G.; Zhao, L.; Cao, S.; Zhu, L.; Ge, Y. Estimation of tropical cyclone wind hazards in coastal regions of China. *Nat. Hazards Earth Syst. Sci.* **2020**, *20*, 1617–1637. [[CrossRef](#)]
10. Vickery, P.J.; Skerlj, P.F.; Twisdale, L.A. Simulation of Hurricane Risk in the U.S. Using Empirical Track Model. *J. Struct. Eng.* **2000**, *126*, 1222–1237. [[CrossRef](#)]
11. Powell, M.; Soukup, G.; Cocke, S.; Gulati, S.; Morisseau-Leroy, N.; Hamid, S.; Dorst, N.; Axe, L. State of Florida hurricane loss projection model: Atmospheric science component. *J. Wind Eng. Ind. Aerodyn.* **2005**, *93*, 651–674. [[CrossRef](#)]
12. James, M.K.; Mason, L.B. Synthetic Tropical Cyclone Database. *J. Waterw. Port Coast. Ocean Eng.* **2005**, *131*, 181–192. [[CrossRef](#)]
13. Emanuel, K.; Ravela, S.; Vivant, E.; Risi, C. A Statistical Deterministic Approach to Hurricane Risk Assessment. *Bull. Am. Meteorol. Soc.* **2006**, *87*, 299–314. [[CrossRef](#)]
14. Lee, K.H.; Rosowsky, D.V. Synthetic hurricane wind speed records: Development of a database for hazard analysis and risk studies. *Nat. Hazards Rev.* **2007**, *8*, 23–34. [[CrossRef](#)]
15. Vickery, P.J.; Wadhera, D.; Twisdale, L.A.; Lavelle, F.M.U.S. Hurricane Wind Speed Risk and Uncertainty. *J. Struct. Eng.* **2009**, *135*, 301–320. [[CrossRef](#)]
16. Li, S.H.; Hong, H.P. Observations on a Hurricane Wind Hazard Model Used to Map Extreme Hurricane Wind Speed. *J. Struct. Eng.* **2015**, *141*, 04014238. [[CrossRef](#)]
17. Li, S.H.; Hong, H.P. Typhoon wind hazard estimation for China using an empirical track model. *Nat. Hazards* **2016**, *82*, 1009–1029. [[CrossRef](#)]
18. Chen, Y.; Duan, Z. A statistical dynamics track model of tropical cyclones for assessing typhoon wind hazard in the coast of southeast China. *J. Wind Eng. Ind. Aerodyn.* **2018**, *172*, 325–340. [[CrossRef](#)]
19. Emanuel, K.A. A fast intensity simulator for tropical cyclone risk analysis. *Nat. Hazards* **2017**, *88*, 779–796. [[CrossRef](#)]
20. Jing, R.; Lin, N. Tropical Cyclone Intensity Evolution Modeled as a Dependent Hidden Markov Process. *J. Clim.* **2019**, *32*, 7837–7855. [[CrossRef](#)]
21. Huang, M.; Wang, Q.; Li, Q.; Jing, R.; Lin, N.; Wang, L. Typhoon wind hazard estimation by full-track simulation with various wind intensity models. *J. Wind Eng. Ind. Aerodyn.* **2021**, *218*, 104792. [[CrossRef](#)]
22. Meng, Y.; Matsui, M.; Hibi, K. An analytical model for simulation of the wind field in a typhoon boundary layer. *J. Wind Eng. Ind. Aerodyn.* **1995**, *56*, 291–310. [[CrossRef](#)]
23. Thompson, E.F.; Cardone, V.J. Practical Modeling of Hurricane Surface Wind Fields. *J. Waterw. Port Coast. Ocean Eng.* **1996**, *122*, 195–205. [[CrossRef](#)]

24. Niu, H.Y.; Liu, M.; Lu, M.; Quan, R.S.; Zhang, L.J.; Wang, J.J. Evaluation of typhoon hazard risk in coastal areas of China in the past 20 years. *Geoscience* **2011**, *6*, 764–768. (In Chinese)
25. Yin, J.; Yin, Z.; Xu, S. Composite risk assessment of typhoon-induced disaster for China's coastal area. *Nat. Hazards* **2013**, *69*, 1423–1434. [[CrossRef](#)]
26. Pielke, R.A., Jr.; Gratz, J.; Landsea, C.W.; Collins, D.; Saunders, M.A.; Musulin, R. Normalized hurricane damage in the United States: 1900–2005. *Nat. Hazards Rev.* **2008**, *9*, 29–42. [[CrossRef](#)]
27. Fang, W.H.; Zhong, X.C.; Qiao, Y.; Lin, W.; Xu, H.; Li, Y. Evaluation of vulnerability of rural housing based on typhoon disaster insurance data in Zhejiang Province. *J. Beijing Norm. Univ.* **2011**, *47*, 409–414. (In Chinese)
28. Chen, Y.L.; Zhu, X.C.; Hu, B.; Gu, X.L. Research on typhoon disaster prediction model in Ningbo based on BP neural network. *J. Atmos. Sci.* **2018**, *41*, 668–675. (In Chinese)
29. Lou, W.P.; Chen, H.Y.; Zheng, F.; Rui, W.U. Economic loss assessment of typhoon disaster based on principal component neural network. *Geogr. Res.* **2009**, *28*, 1243–1254. (In Chinese)
30. Ying, M.; Zhang, W.; Yu, H.; Lu, X.; Feng, J.; Fan, Y.; Zhu, Y.; Chen, D. An Overview of the China Meteorological Administration Tropical Cyclone Database. *J. Atmos. Ocean. Technol.* **2014**, *31*, 287–301. [[CrossRef](#)]
31. Schilling, R.J.; Carroll, J.J.J.; Al-Ajlouni, A.F. Approximation of nonlinear systems with radial basis function neural networks. *IEEE Trans. Neural Netw.* **2001**, *12*, 1–15. [[CrossRef](#)]
32. Huang, M.F.; Li, Q.; Xu, H.W.; Lou, W.J.; Lin, N. Non-stationary statistical modeling of extreme wind speed series records with exposure correction. *Wind Struct.* **2018**, *26*, 129–146.
33. Vickery, P.J.; Wadhera, D. Statistical models of Holland pressure profile parameter and radius to maximum winds of hurricanes from flight-level pressure and H* Wind data. *J. Appl. Meteorol. Climatol.* **2008**, *47*, 2497–2517. [[CrossRef](#)]
34. GB50009-2012; Building Structure Load Code. China Standards Press: Beijing, China, 2012. (In Chinese)